Accepted Manuscript

Title: Pressure-Controlled Chemical Vapor Deposition of Graphene as Catalyst for Solar Hydrogen Evolution Reaction

Authors: Chih-Pin Han, Chih-Jung Chen, Chen-Chih Hsu, Anirudha Jena, Ho Chang, Nai-Chang Yeh, Shu-Fen Hu, Ru-Shi Liu

PII: S0920-5861(18)31006-X
DOI: https://doi.org/10.1016/j.cattod.2019.01.001
Reference: CATTOD 11872

To appear in: *Catalysis Today*

Received date: 1 October 2018
Revised date: 20 December 2018
Accepted date: 2 January 2019

Please cite this article as: Han C-Pin, Chen C-Jung, Hsu C-Chih, Jena A, Chang H, Yeh N-Chang, Hu S-Fen, Liu R-Shi, Pressure-Controlled Chemical Vapor Deposition of Graphene as Catalyst for Solar Hydrogen Evolution Reaction, *Catalysis Today* (2019), https://doi.org/10.1016/j.cattod.2019.01.001

Pressure-Controlled Chemical Vapor Deposition of Graphene as Catalyst for Solar Hydrogen Evolution Reaction

Chih-Pin Han[a], Chih-Jung Chen[a], Chen-Chih Hsu[b], Anirudha Jena[a,c], Ho Chang[c], Nai-Chang Yeh[b,*], Shu-Fen Hu[d,*], Ru-Shi Liu[a,c,*]

[a] Department of Chemistry, National Taiwan University, Taipei 106, Taiwan

[b] Department of Physics, California Institute of Technology, Pasadena, California 91125, USA

[c] Department of Mechanical Engineering and Graduate Institute of Manufacturing Technology, National Taipei University of Technology, Taipei 106, Taiwan

[d] Department of Physics, National Taiwan Normal University, Taipei 116, Taiwan

Corresponding authors

E-mail addresses: ncyeh@caltech.edu (N. C. Yeh), sfhu.hu@ntnu.edu.tw (S. F. Hu), rsliu@ntu.edu.tw (R. S. Liu).

Graphical abstract

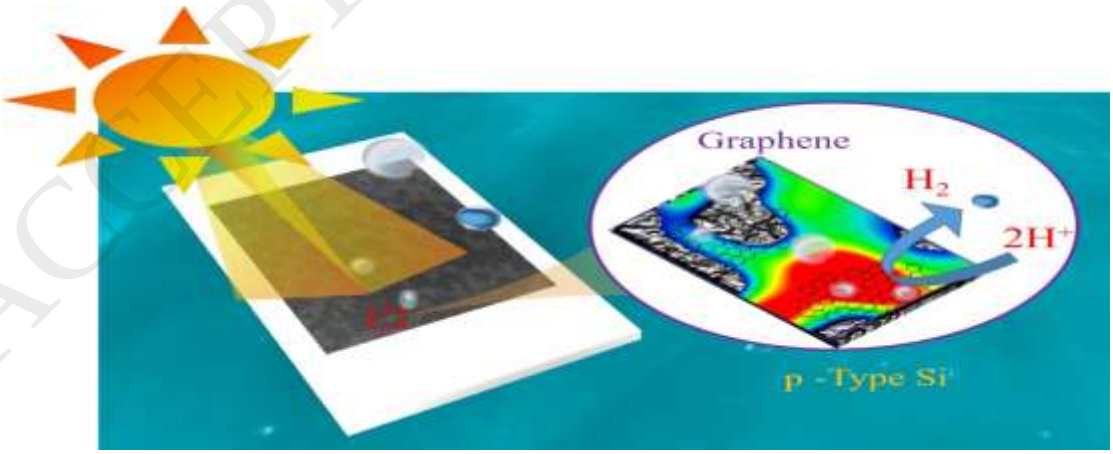

Research Highlights

- Photocatalyst Water splitting as clear energy for hydrogen evolution reaction.
- Silicon earth-abound material as substrate photoabsorber absorbs wide range solar light.
- Carbon material low cost, high chemical stability for water splitting.
- Graphene synthesis by different methods, next though to transferred to silicon by polymer substrate as a catalyst layer.

ABSTRACT

In the present report, graphene-based catalysts on silicon substrate have been examined as the photocathode for solar hydrogen evolution reaction (HER). Mono-layered graphene has been synthesized through low-pressure chemical vapor deposition (LPCVD), whereas multi-layered graphene has been synthesized by atmospheric pressure chemical vapor deposition (APCVD). Copper foil is used as the substrate. The graphene layer on Cu foil subsequently transferred on to silicon photoabsorber using poly(methyl-2-methylpropenoate) (PMMA). At the initial linear sweep voltammetry (LSV) scan, LPCVD-synthesized graphene-Si (LPCVD-Si) electrode showed an onset potential of −0.65 V and photocurrent of −4.31 mA cm^{-2} (at −0.385 V). On the contrary, the onset potential and photocurrent of APCVD-prepared graphene-Si (APCVD-Si) photocathode are −0.36 V and −28.28 mA cm^{-2} (at −0.385 V), respectively. After the 130^{th} LSV scan, the onset potential and photocurrent of LPCVD-Si improved to −0.39 V and −13.28 mA cm^{-2} (at −0.385 V), respectively. In addition, the onset potential and

photocurrent of APCVD-Si photocathode at the LSV 130th scan are enhanced to −0.36 V and −28.28 mA cm^{-2} (at −0.385 V), respectively. The graphene sample grown via LPCVD-Si show stable performance whereas, the graphene obtained via APCVD-Si have higher photocurrent poor stability.

Keywords: Silicon, Graphene, Hydrogen evolution reaction (HER), Metal-free catalyst Photoelectrochemical cell

1. Introduction

Greenhouse gases have increased by abusing oil and coal, which contributed to global warming. Consequently, environmentally-friendly energy, such as solar energy, has been rapidly developed [1-7]. In 1972, splitting water using TiO_2 solar conversion system to generate hydrogen gas has been investigated by Honda and Fujishima [8]. Hydrogen gas is the only alternative fuel stored with almost unlimited amounts in the ocean. It is more abundant and environmentally clean compared with nonrenewable carbon-based fossil fuels. Accordingly, numerous researches on hydrogen storage and generator systems based on splitting water are devoted for the past decades. Moreover, electrochemical/photoelectrochemical-driven hydrogen evolution reaction (HER) has been regarded as a promising method for producing hydrogen gas.

A variety of semiconductor-based materials have been developed as photocatalysts for solar photoelectrolysis. Nevertheless, silicon is the candidate of photocathode material for HER due to its band edge near ca. −0.46 V vs. NHE reach to hydrogen formation energy and short band gap (1.1 eV) easy to form an electron and electron-hole [9, 10]. However, low HER kinetics on pristine silicon contributed to low photocatalytic performance. Therefore, noble metal Pt as co-catalyst is decorated with silicon for enhancing the efficiency and also decreased the electron-hole pair recombination [11]. However, high-cost noble metal limits their wide range of uses and their applications for commercial because of their shortage worldwide [12]. Another restriction of using silicon for water splitting is the easy oxidation to SiO_2 after exposure to the electrolyte. SiO_2 is an electric insulator that reduces the photogenerated carriers to migrate to the surface for reacting with redox couples in the electrolyte [13]. The use of methyl group halogenation/alkylation to silicon surface as a hydrophobic passivation layer can be a strategy to prevent silicon oxidation [14, 15].

Carbon-based materials are widely applied as electrocatalysts because of low-cost and high chemical stability in HER, [16] OER [17], and ORR [18]. Graphene, constructed by carbon sp^2 orbital, is ultrathin and highly conductive. Therefore, many scientists devoted to its research [19]. Some reports claimed that graphene is used in touch-screen displays, [20] photonics, optoelectronics, [21] and storage devices [22-

25]. In previous works, doping heteroatoms (such as N and P atoms) on carbon material caused the valence orbital energy levels to induce a synergistically enhanced reactivity toward HER [26], and N, P-heteroatom-doped graphene matrix improved the HER activity [27]. Nitrogen-doped graphene directly grown on graphitic-carbon nitride also exhibited high HER activity [28]. Zhang et al. tri-doped N, P, and F atoms into graphene as a catalyst for electrochemical water splitting [29]. In 2013, Sim et al. used N-doped monolayer graphene catalyst on silicon as the photocathode for HER [30]. To further enhance the performance, N-doped graphene quantum sheets are prepared on silicon nanowire as photocathodes for solar-driven HER [31]. In 2017, this researching group investigated the graphene with 1–5 layers as catalysts on silicon photocathode for HER [32].

Here, graphene-modified silicon photocathodes are prepared for water splitting, as shown in Scheme 1. We used LPCVD and APCVD to fabricate single and multi-layered graphene, respectively. After utilizing poly(methyl 2-methylpropenoate) (PMMA) to transfer graphene on silicon, we abbreviated these photocathodes as LPCVD-Si and APCVD-Si. Simple methods are applied to synthesize two different types of graphene and served as a catalyst layer. After the 130^{th} linear sweep voltammetry (LSV) scans, the onset potential and photocurrent of LPCVD-Si electrode are enhanced to −0.39 V and −13.28 mA cm^{-2} (at −0.385 V), respectively. Besides, the onset potential and

photocurrent of APCVD-Si photocathode at LSV 130th scans are separately increased to −0.36 V and −28.28 mA cm^{-2} (at −0.385 V). We propose that the gas bubble damaged the graphene surface and generated the defects, which served as HER active sites for increasing the current after several LSV scans. Therefore, the LPCVD- and APCVD-prepared graphene are potential metal-free catalyst materials.

2. Experimental

2.1 Modification of Si wafer as substrate for deposition of graphene

Boron-doped p-type silicon wafers (resistivity: 1–25 Ω cm, orientation: (100), diameter: 150 mm, thickness: 675±25 μm) were used to fabricate electrodes. The back side is thinned up to a total thickness of 325±5 μm by chemical–mechanical polishing. Then E-gun was used to deposit aluminum on the back side with a thickness of 500 nm. The aluminum back silicon wafers were annealed at 400 °C for 30 min to improve the silicon and aluminum bonding. The back side was conducted with copper wire. This electrode is prepared for further use.

2.2 Fabrication of APCVD graphene

Copper foil (5 × 3 cm^2) with thickness of 0.025 mm (Alfa Aesar) was used as substrate. Multi-layered graphene was deposited using APCVD. Use of metallic substrates, such as copper, is essential for the growth of graphene owing to the

capability of absorbing and decomposing hydrocarbons like CH_4 [33]. The copper foil surface was blown by N_2 gas before deposition. Then, the copper foil was placed in a quartz tube and vacuumed until 3 mTorr for a clean the quartz tube. Then it was heated to 900 °C for 60 min with H_2 flowing at a rate of 10 sccm and Ar as carrier gas at a rate of 50 sccm. The temperature was maintained for 30 min with H_2 flowing at 10 sccm and Ar at 50 sccm. Then methane was added into the tube (5 sccm CH_4, 10 sccm H_2, and 50 sccm Ar) for 30 min. The pressure during the process was 760 Torr. The heater was turned off and removed from the quartz tube quickly after 30 min. The as-heated samples naturally cooled down to room temperature.

2.3 Fabrication of LPCVD graphene

The single-layered graphene was synthesized by the LPCVD method, following the previously reported method [34]. Copper foil (5×3 cm^2) was blown by N_2 gas to clean the surface. Then, the copper foil was placed in a quartz tube and pumped down until 3 mTorr to clean the quartz tube. Next, it was heated to 1000 ℃ for 60 min with the H_2 flowing rate of 10 sccm and the Ar carrier gas flow rate of 50 sccm. Annealing was maintained for 30 min with flowing H_2 at 10 sccm and Ar carrier gas at 50 sccm. Then, a gas mixture (15 sccm CH_4, 10 sccm H_2, and 50 sccm Ar carrier gas) was flowed for 90 min at under 10 mTorr. The pressure was under 40 mTorr. The heater was turned off and removed from the quartz tube quickly after 90 min, and the as-heated samples

naturally cooled down to room temperature.

2.4 Fabrication of multi-/monolayered graphene deposited silicon wafer

PMMA was used as a support layer to transfer graphene to the target silicon. the graphene-deposited copper foil was spin-coated with PMMA and named PMMA/graphene/Cu [35, 36]. The PMMA photoresist solution was as prepared with a concentration of 4% in anisole (molecular weight 950 A4, MicroChem Corp.) Shaking was avoided to prevent the formation of air bubbles inside the bottle. The bubble influences the PMMA thin film contact with graphene. Stairs spin-coating speed steps were used in the graphene/Cu from 1000 rpm to 2000 rpm for 30 s. The substrates were post-baked at 180 ^{o}C for 60 s on a hot plate after spin coating.

Then the copper substrate was etched using an etchant solution (0.1 M $FeCl_3$, Sigma–Aldrich). The copper foil was etched using the etchant solution. The thin film (PMMA/graphene) drifted on the surface of the solution. The PMMA/graphene was transferred to deionized water several times in order to clean the etchant solution. The silicon wafer was pretreated with 10% HF for 30 s. The silicon wafers we prepared (1 × 1 cm^{-2}) substrate was then used to pick up the PMMA/graphene from the deionized water, forming PMMA/graphene/silicon. The PMMA/graphene/silicon was dried under ambient conditions for 24 h. The PMMA film was removed in warm acetone for 120

s[37]. Finally, we prepared the wafer LPCVD-Si and APCVD-Si.

2.5 Photoelectrochemical measurement

The aluminum back silicon electrode produced as prepared above are bonded with copper wire by Ag paste and oven dried at 60 °C for 2 h. The electrode was coated by insulating epoxy (AB glue) on the photocathode to avoid the dark current and short circuit. The photoelectrochemical cell was carried out in a three-electrode system. The entire system is surrounded by water circulation and maintained at 25 °C. The working electrode was prepared as previously described. Graphite roll was used as the counter electrode and Ag/AgCl as a reference electrode. The electrolyte used was 250 mL of aqueous solution of 0.5M H_2SO_4. Xenon lamp equipped with Air Mass 1.5 Global glass filter was used, and the light intensity was 100 mW cm^{-2} as constant. Eco Chemie AUTOLAB and The Netherlands and General Purpose Electrochemical System software were used to recording and analyze LSVs, chronoamperometry, and transient photocurrent curve. The LSV measurements were obtained from 0.556 V to −0.78 V with a scan rate of 20 mV s^{-1}. Chronoamperometry and transient photocurrent curve were performed at −0.385 V vs RHE.

2.6 Characterization

The morphologies of the LPCVD-Si and APCVD-Si were investigated by scanning electron microscopy (SEM, ZEISS ΣIGMA Essential) with 15.0 kV. The LPCVD-Si

and APCVD-Si surface graphene stretching vibration modes were evaluated using Raman spectrometers (DXR microscope, Thermo) with 532 nm laser. Bruker D2 PHASER X-ray diffraction (XRD) analyzer with Cu Kα as a source of radiation was used to determine the crystallization of the LPCVD-Si and APCVD-Si before and after LSVs.

3. Result and discussion

The scanning electron microscopy (SEM) images of LPCVD-Si and APCVD-Si are shown in Fig. 1. The SEM image in the Fig. 1a shows the single-layered graphene obtained through LPCVD transferred on to the silicon wafer [38], and in Fig. 1b**,** the multi-layered graphene obtained through APCVD, after transferred on to the silicon wafer [39]. The SEM images clearly show successful transfer of large-area graphene layers on silicon by using PMMA. The graphene films obtained via LPCVD and APCVD transferred on to silicon are further characterized by Raman spectra (Fig. 1c and d), which provides information on the graphitization of different samples. Peaks in the Raman spectra are purely generated from graphene without any side products. The G band ration to the 2D band of graphene materials is applied to evaluate the layer numbers [40]. If the G to 2D band ratio is near 0.5, graphene successfully formed a single-layer [41]. If G and 2D band ratio are near 1, graphene is double layered. In addition, as the G to 2D band ratio is higher than 1, these graphene films formed a

multi-layer. In the present work, the E_{2g} vibrational modes of sp^2 carbon about ring and chain exhibited the G band at 1577.9 cm^{-1}, whereas the carbon material edge about the A_{1g} mode of the sp^3 at 1344.5 cm^{-1}, which contrasted to the D band. In addition, the secondary vibration scattering of phonons at regional boundaries to the 2D peak is observed at 2739 cm^{-1} [42, 43]. The single- and multi-layered graphene, respectively prepared by LPCVD and APCVD, are observed through Raman spectrometry. The G to 2D band intensity ratio of LPCVD graphene at ~0.5 without D band generation are a single-layer graphene. When the G to a 2D band intensity ratio of APCVD graphene are higher than 1, we suspect a multi-layered graphene (3–4 layers). Raman mapping on the graphene films shown in Fig S1 are recorded to further confirm the graphene layers. Fig. S1a, the LPCVD graphene show the single layer. APCVD shows the multi-layered in Fig. S1b. The mapping can analyze the area of the thin film thickness[44]. Moreover, D band, which served as defect structures on graphene layers, are observed in the Raman spectrum of APCVD graphene. Fig. S2 and S3 show the high-resolution transmission electron microscope (HRTEM) image of LPCVD and APCVD, respectively [45]. In Fig. S2a, the TEM image exhibit the LPCVD nanosheet morphology. The TEM image of APCVD shows much thick layer in Fig. S3a. HRTEM can provide the evidence about the APCVD graphene which has a multi-layer structure in Fig. S2b. In Fig. S3b, the LPCVD graphene only display few layers in the image.

Both LPCVD and APCVD of selected area electron diffraction (SAED) relative with the previous report in Fig. S2c and S3c [45]. The lattice planes show the (100) and (110) in this area. Therefore, the Raman, HRTEM and SAED image analyzation demonstrate the graphene have been syntheses by different pressure parameter. Fig. 2 shows the X-ray diffraction (XRD) spectra of LPCVD-Si and APCVD-Si photocathodes before the LSV measurements and after the 190th LSV scans. The diffraction peaks at 2 theta values of 69° corresponded to the Miller index (400) of the silicon substrate [46]. No graphene peaks are observed because of its low loading amount and crystallinity with respect to Si substrate. Furthermore, no by-product peaks are observed in the XRD spectra, indicating that the graphene layer successfully transferred on silicon.

LSV measurements are carried out successively till 190th scan to analyze the durability of graphene-decorated silicon photocathodes. The onset potential and photocurrent of graphene-modified silicon electrodes are shown in Fig. 3. The result shows that their photocurrent increased with LSV scans and the maximum photocurrent are achieved at the 130th scan. This evidence indicates the catalyst efficiency is influenced by LSV scans. At the 130th scan, the LPCVD-Si onset potential is −0.39 V, and the photocurrent is −13.28 mA cm^{-2} at −0.385 V, as shown in Fig. 3a. The result indicates that the photocurrent is enhanced by LSV scans. We suspect that the material has changed. In Fig. 3c, the LSV showed that the 130th scan of APCVD-Si exhibited

considerably higher onset potential of −0.36 V and larger photocurrent at −28.28 mA cm^{-2} at −0.385 V. This phenomenon is supported by the SEM images that are used to analyze the surface change. SEM is applied to evaluate the morphology variations of graphene-decorated silicon photocathodes after continuous LSV scans. Figs. 4a and b show the SEM image of LPCVD-Si photocathode and the morphology at the 130^{th} and 190^{th} scans. In the initial stage, graphene with the complete sheet is deposited on a silicon substrate, whereas its surface showed partially broken parts at the 130^{th} scan (Fig. 4a). After LSV 190^{th} scans, no graphene existed on the silicon surface. On the other hand, this phenomenon is also observed from APCVD-Si photocathode, as shown in Figs. 4c and d. We suspect that the surface defect provided the active side and largely influence the photocurrent. In a previous report, the graphene layer is shown to enhance the photocurrent [32]. This result corresponds with those of the LSVs, which is the reason for the considerably higher photocurrent of APCVD-Si.

Raman spectra are recorded to further understand the surface change on graphene-modified silicon electrodes during LSV scans. In Fig. 5, Raman spectra show the variations of graphene peaks after LSV scans. At the initial stage, the LPCVD and APCVD graphene are single- and multi-layered, respectively. At the 130^{th} LSV scans, the Raman spectra show the D and 2D band change. The D band of LPCVD graphene at 1331 cm^{-1} and the 2D band of APCVD graphene decreased, as shown in Fig. 5a. The

Raman mapping provides in Fig. S4. Fig. S4a shows the LPCVD-Si before LSV's mapping. After 130th scans, the Raman mapping about defects shows in Fig. S4b. We suggest the defect which produces by gas bubble damage the surface. After the LSV 190th scan, Raman spectra indicate the silicon surface had no graphene thin films anymore. During the successive LSV measurements, the hydrogen gas bubbles are violently generated on graphene-deposited silicon photocathode materials. Based on the Raman spectroscopic studies, we conjecture that the LSV scans produced the bubbles to destroy the graphene surface. This result is also observed in APCVD-Si, as shown in Fig. 5b. Fig. 6 shows the XRD of LPCVD-Si and APCVD-Si photocathodes after the 190th LSV scans. The diffraction peaks at 2 theta values of 69° corresponded to the Miller index (400) of the silicon substrate indicating the structural integrity.

Chronoamperometry is conducted at −0.385 V under solar illumination. Figs. 7a and 7c respectively show three photocurrent stages of the LPCVD-Si and APCVD-Si electrodes during the 10 h chronoamperometric measurement. At the first stage, the photocurrent is low because the silicon surface is still covered with complete graphene. At the second stage, the current density increased because the graphene surface is damaged by gas bubbles [30]. Finally, graphene detached from silicon photoabsorber under violent HER condition, and silicon is exposed with the electrolyte. These results contributed to photocatalytic degradation. Special attention is paid on APCVD-Si,

which is particularly unstable during the chronoamperometry and easy to demold. The result shows the APCVD-Si is more unstable than LPCVD-Si.

Transient photoresponse measurements of LPCVD-Si and APCVD-Si electrodes are also performed under the light on and off conditions, as shown in Figs. 7b and 7d. The potential is set at −0.385 V (vs RHE) for the solar light open and close every 30 s using a cardboard. No sharp overshoot is observed when the light is turned on and off. We suggested that the carriers of the electrodes easily transferred to the electrolyte and reduced recombination. This indicates that the graphene is a good electronic conductor.

4. Conclusions

We developed the LPCVD and APCVD graphene as catalysts for water splitting. Therefore, the LPCVD- and APCVD-prepared graphene are found to be a potential metal-free catalyst material. The APCVD-Si showed higher photocurrent at the beginning, while LPCVD-Si showed better stability. The photocurrent of graphene-Si electrodes both increased with LSV scans due to the surface change but finally gradually reduced because of the detachment. Especially at the 130^{th} scan, the onset potential and photocurrent of LPCVD-Si are −0.39 V and −13.28 mA cm^{-2} at −0.385 V, respectively. On the other hand, the onset potential and photocurrent at the 130^{th} scan of APCVD-Si are −0.36 V and −28.28 mA cm^{-2} at −0.385 V, respectively. Moreover,

the activation of the single- and multi-layered catalyst for water splitting increased the photocurrent depending on time. The graphene decomposed into sheets and enhanced the photocurrent during PEC measurements while exposing more silicon surface to the electrolyte, which resulted in the oxidation and photocatalytic degradation. This work provided a method of synthesizing large-area graphene and transferring to a silicon wafer as a catalyst for water splitting.

Acknowledgment

We thank the financial support from the Ministry of Science and Technology (Contract Nos. MOST 106-2112-M-003-007-MY3 and MOST 107-2113-M-002-008-MY3).

References

[1] G. Xie, K. Zhang, B. Guo, Q. Liu, L. Fang, J.R. Gong, Adv. Mater., 25 (2013) 3820-3839.
[2] R.E. Blankenship, D.M. Tiede, J. Barber, G.W. Brudvig, G. Fleming, M. Ghirardi, M.R. Gunner, W. Junge, D.M. Kramer, A. Melis, T.A. Moore, C.C. Moser, D.G. Nocera, A.J. Nozik, D.R. Ort, W.W. Parson, R.C. Prince, R.T. Sayre, Science, 332 (2011) 805-809.
[3] I. Roger, M.A. Shipman, M.D. Symes, Nat Rev Chem., 1 (2017) 0003.
[4] M.G. Walter, E.L. Warren, J.R. McKone, S.W. Boettcher, Q. Mi, E.A. Santori, N.S. Lewis, Chem. Rev., 110 (2010) 6446-6473.
[5] X. Ji, B. Liu, X. Ren, X. Shi, A.M. Asiri, X. Sun, ACS Sustainable Chem. Eng., 6 (2018) 4499-4503.
[6] Z. Wang, X. Ren, Y. Luo, L. Wang, G. Cui, F. Xie, H. Wang, Y. Xie, X. Sun, Nanoscale, 10 (2018) 12302-12307.
[7] Y. Ji, L. Yang, X. Ren, G. Cui, X. Xiong, X. Sun, ACS Sustainable Chem. Eng., 6 (2018) 11186-11189.
[8] A. Fujishima, K. Honda, Nature, 238 (1972) 37.
[9] X. Chen, S. Shen, L. Guo, S.S. Mao, Chem. Rev., 110 (2010) 6503-6570.
[10] A. Kudo, Y. Miseki, Chem. Soc. Rev., 38 (2009) 253-278.
[11] S.W. Boettcher, E.L. Warren, M.C. Putnam, E.A. Santori, D. Turner-Evans, M.D. Kelzenberg, M.G. Walter, J.R. McKone, B.S. Brunschwig, H.A. Atwater, N.S. Lewis, J. Am. Chem. Soc., 133 (2011) 1216-1219.
[12] J.R. McKone, N.S. Lewis, H.B. Gray, Chem. Mater., 26 (2014) 407-414.
[13] B. Seger, T. Pedersen, A.B. Laursen, P.C.K. Vesborg, O. Hansen, I. Chorkendorff, J. Am. Chem. Soc., 135 (2013) 1057-1064.
[14] L.E. O'Leary, M.J. Rose, T.X. Ding, E. Johansson, B.S. Brunschwig, N.S. Lewis, J. Am. Chem. Soc., 135 (2013) 10081-10090.
[15] H. Haick, P.T. Hurley, A.I. Hochbaum, P. Yang, N.S. Lewis, J. Am. Chem. Soc., 128 (2006) 8990-8991.
[16] Y. Li, H. Wang, L. Xie, Y. Liang, G. Hong, H. Dai, J. Am. Chem. Soc., 133 (2011) 7296-7299.
[17] J. Tian, Q. Liu, A.M. Asiri, K.A. Alamry, X. Sun, ChemSusChem, 7 (2014) 2125-2130.
[18] C. Hu, L. Dai, Adv. Mater., 29 (2017) 1604942.
[19] A.H. Castro Neto, F. Guinea, N.M.R. Peres, K.S. Novoselov, A.K. Geim, REV MOD PHYS, 81 (2009) 109-162.

[20] S. Bae, H. Kim, Y. Lee, X. Xu, J.S. Park, Y. Zheng, J. Balakrishnan, T. Lei, H. Ri Kim, Y.I. Song, Y.J. Kim, K.S. Kim, B. Özyilmaz, J.H. Ahn, B.H. Hong, S. Iijima, Nat. Nanotech., 5 (2010) 574.
[21] F. Bonaccorso, Z. Sun, T. Hasan, A.C. Ferrari, Nat Photonics., 4 (2010) 611.
[22] B. Xie, C. Yang, Z. Zhang, P. Zou, Z. Lin, G. Shi, Q. Yang, F. Kang, C.P. Wong, ACS Nano, 9 (2015) 5636-5645.
[23] X. Cao, Z. Yin, H. Zhang, Energy Environ. Sci., 7 (2014) 1850-1865.
[24] J. Zhu, D. Yang, Z. Yin, Q. Yan, H. Zhang, Small, 10 (2014) 3480-3498.
[25] Z. Yin, J. Zhu, Q. He, X. Cao, C. Tan, H. Chen, Q. Yan, H. Zhang, Adv. Energy Mater., 4 (2014) 1300574.
[26] Y. Zheng, Y. Jiao, L.H. Li, T. Xing, Y. Chen, M. Jaroniec, S.Z. Qiao, ACS Nano, 8 (2014) 5290-5296.
[27] J. Zhang, L. Qu, G. Shi, J. Liu, J. Chen, L. Dai, Angew. Chem. Int. Ed., 55 (2016) 2230-2234.
[28] Y. Zheng, Y. Jiao, Y. Zhu, L.H. Li, Y. Han, Y. Chen, A. Du, M. Jaroniec, S.Z. Qiao, Nat. Commun., 5 (2014) 3783.
[29] J. Zhang, L. Dai, Angew. Chem. Int. Ed., 55 (2016) 13296-13300.
[30] U. Sim, T.-Y. Yang, J. Moon, J. An, J. Hwang, J.-H. Seo, J. Lee, K.Y. Kim, J. Lee, S. Han, B.H. Hong, K.T. Nam, Energy Environ. Sci., 6 (2013) 3658-3664.
[31] U. Sim, J. Moon, J. An, J.H. Kang, S.E. Jerng, J. Moon, S.-P. Cho, B.H. Hong, K.T. Nam, Energy Environ. Sci., 8 (2015) 1329-1338.
[32] U. Sim, J. Moon, J. Lee, J. An, H.Y. Ahn, D.J. Kim, I. Jo, C. Jeon, S. Han, B.H. Hong, K.T. Nam, ACS Appl. Mater. Interfaces, 9 (2017) 3570-3580.
[33] C. Mattevi, H. Kim, M. Chhowalla, J. Mater. Chem., 21 (2011) 3324-3334.
[34] X. Li, W. Cai, J. An, S. Kim, J. Nah, D. Yang, R. Piner, A. Velamakanni, I. Jung, E. Tutuc, S.K. Banerjee, L. Colombo, R.S. Ruoff, Science, 324 (2009) 1312-1314.
[35] A. Guermoune, T. Chari, F. Popescu, S.S. Sabri, J. Guillemette, H.S. Skulason, T. Szkopek, M. Siaj, Carbon, 49 (2011) 4204-4210.
[36] N.G. Semaltianos, Microelectron. J., 38 (2007) 754-761.
[37] V. Miseikis, S. Xiang, S. Roddaro, S. Heun, C. Coletti, in: V. Morandi, L. Ottaviano (Eds.) GraphITA : Selected papers from the Workshop on Synthesis, Characterization and Technological Exploitation of Graphene and 2D Materials Beyond Graphene, Springer International Publishing, Cham, 2017, pp. 113-124.
[38] A.T. Murdock, A. Koos, T.B. Britton, L. Houben, T. Batten, T. Zhang, A.J. Wilkinson, R.E. Dunin-Borkowski, C.E. Lekka, N. Grobert, ACS Nano, 7 (2013) 1351-1359.
[39] Y. Hao, M.S. Bharathi, L. Wang, Y. Liu, H. Chen, S. Nie, X. Wang, H. Chou, C. Tan, B. Fallahazad, H. Ramanarayan, C.W. Magnuson, E. Tutuc, B.I. Yakobson, K.F.

McCarty, Y.-W. Zhang, P. Kim, J. Hone, L. Colombo, R.S. Ruoff, Science, 342 (2013) 720-723.
[40] A. Das, B. Chakraborty, A.K. Sood, Bull. Mater. Sci., 31 (2008) 579-584.
[41] A.C. Ferrari, J. Robertson, Phys. Rev. B, 64 (2001) 075414.
[42] S. Niyogi, E. Bekyarova, M.E. Itkis, H. Zhang, K. Shepperd, J. Hicks, M. Sprinkle, C. Berger, C.N. Lau, W.A. deHeer, E.H. Conrad, R.C. Haddon, Nano Lett., 10 (2010) 4061−4066.
[43] A.C. Ferrari, J.C. Meyer, V. Scardaci, C. Casiraghi, M. Lazzeri, F. Mauri, S. Piscanec, D. Jiang, K.S. Novoselov, S. Roth, A.K. Geim, Phys. Rev. Lett., 97 (2006) 187401.
[44] D. Graf, F. Molitor, K. Ensslin, C. Stampfer, A. Jungen, C. Hierold, L. Wirtz, The European Physical Journal Special Topics, 148 (2007) 171-176.
[45] G. Wang, J. Yang, J. Park, X. Gou, B. Wang, H. Liu, J. Yao, J. Phys. Chem. C, 112 (2008) 8192-8195.
[46] M. Nieminen, S. Lehto, L. Niinistö, J. Mater. Chem., 11 (2001) 3148-3153.

Figures and Captions:

Fig. 1. SEM images of (a) LPCVD-Si materials and (b) APCVD-Si materials; Raman spectra of (c) LPCVD-Si materials and (d) APCVD-Si materials.

Fig. 2. XRD of various LPCVD-Si and APCVD-Si. The inset is the XRD of the bare Si electrode.

Fig. 3. (a) Linear-sweep voltammograms of LPCVD-Si electrodes. (b) Onset potential and photocurrent of LPCVD-Si electrodes. (c) Linear-sweep voltammograms of APCVD-Si electrodes. (d) Onset potential and photocurrent of APCVD-Si electrodes.

Fig. 4. (a) Chronoamperometry of LPCVD-Si electrodes under solar irradiation at −0.385 V vs. RHE.(b) Transient curve of the photocurrent from LPCVD-Si electrodes when the light was turned on and turned off at −0.385 V vs. RHE. (c) Chronoamperometry of APCVD-Si electrodes under solar irradiation at −0.385 V vs. RHE. (d) Transient curve of the photocurrent from APCVD-Si electrodes when the light was turned on and turned off at −0.385 V vs. RHE.

Fig. 5. SEM of (a) LPCVD-Si materials after the 130^{th} scans. (b) LPCVD-Si materials after the 190^{th} scans. (c) APCVD-Si materials after the 130^{th} scans. (d) APCVD-Si materials after the 190^{th} scans.

Fig. 6. XRD of various LPCVD-Si and APCVD-Si after the 130^{th} scans. The inset is the XRD of the bare Si electrode.

Fig. 7. Raman of (a) LPCVD-Si materials after the 130^{th} and 190^{th} scans. (d) APCVD-Si material after the 130^{th} and 190^{th} scans.

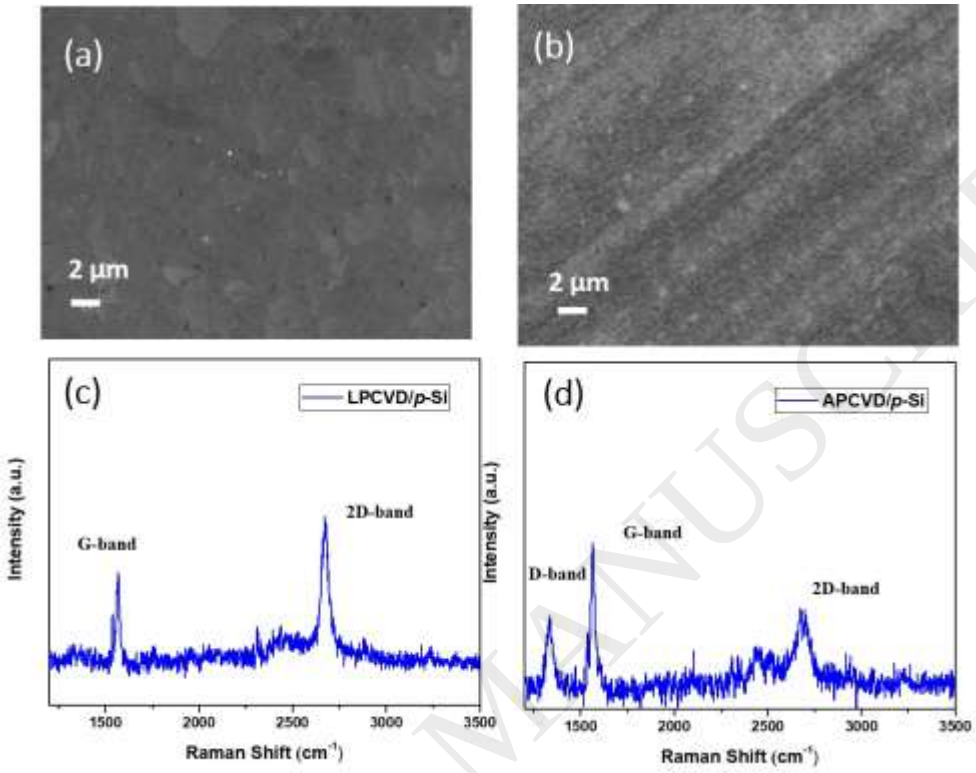

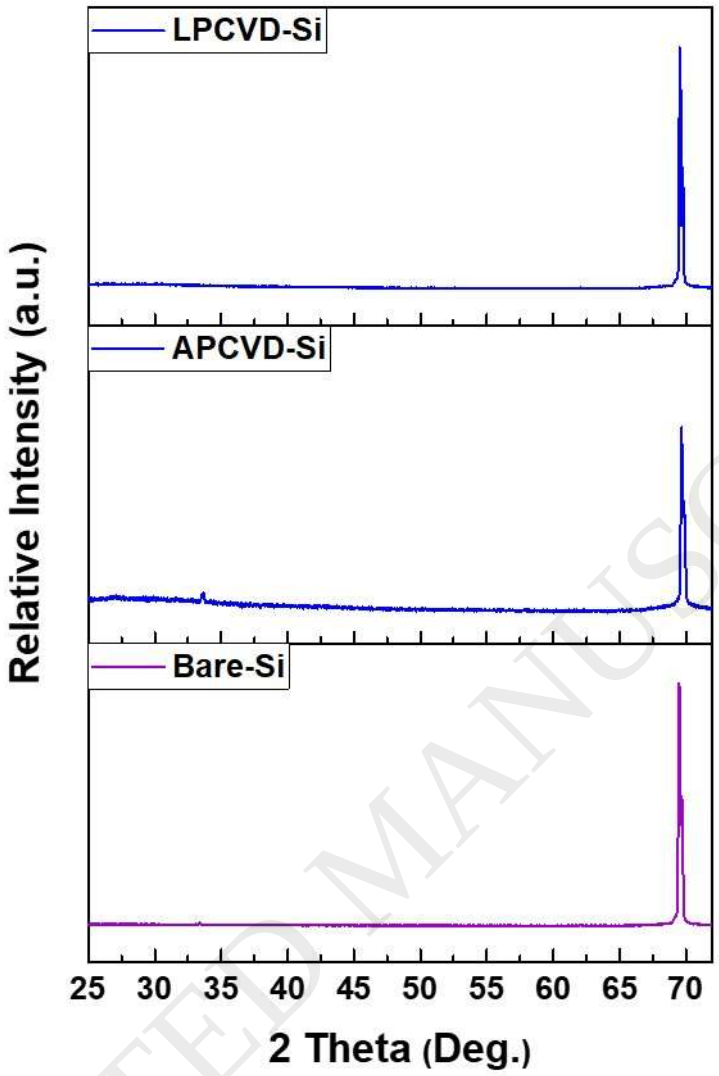

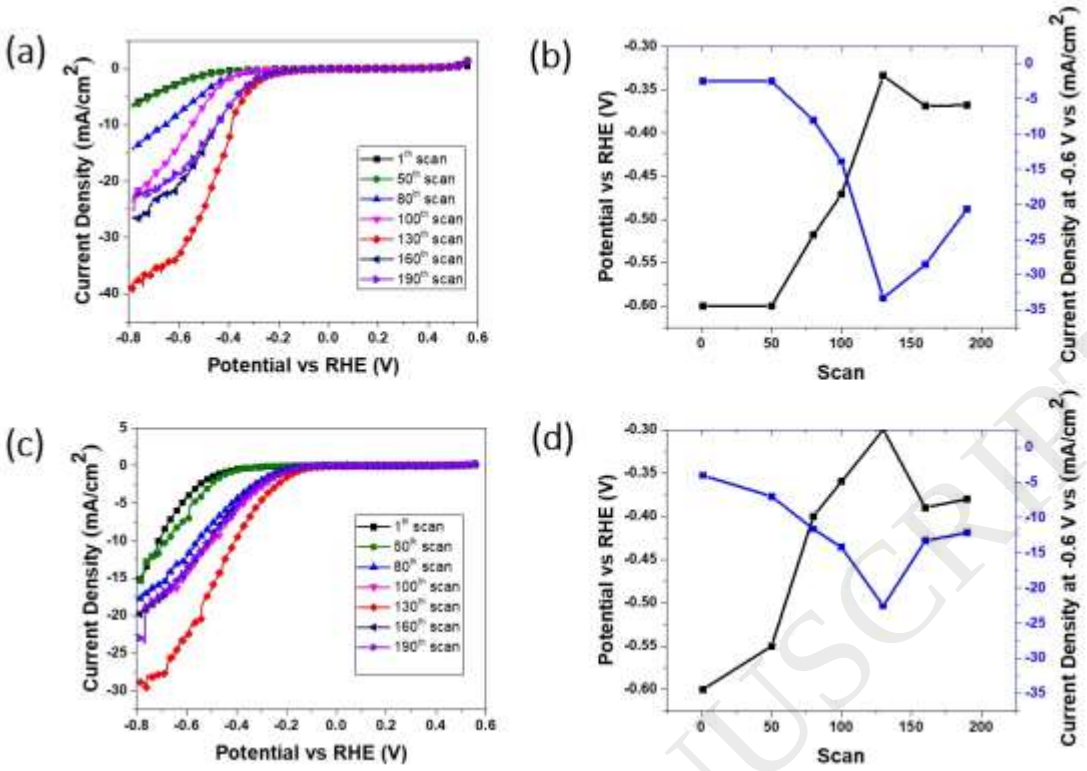

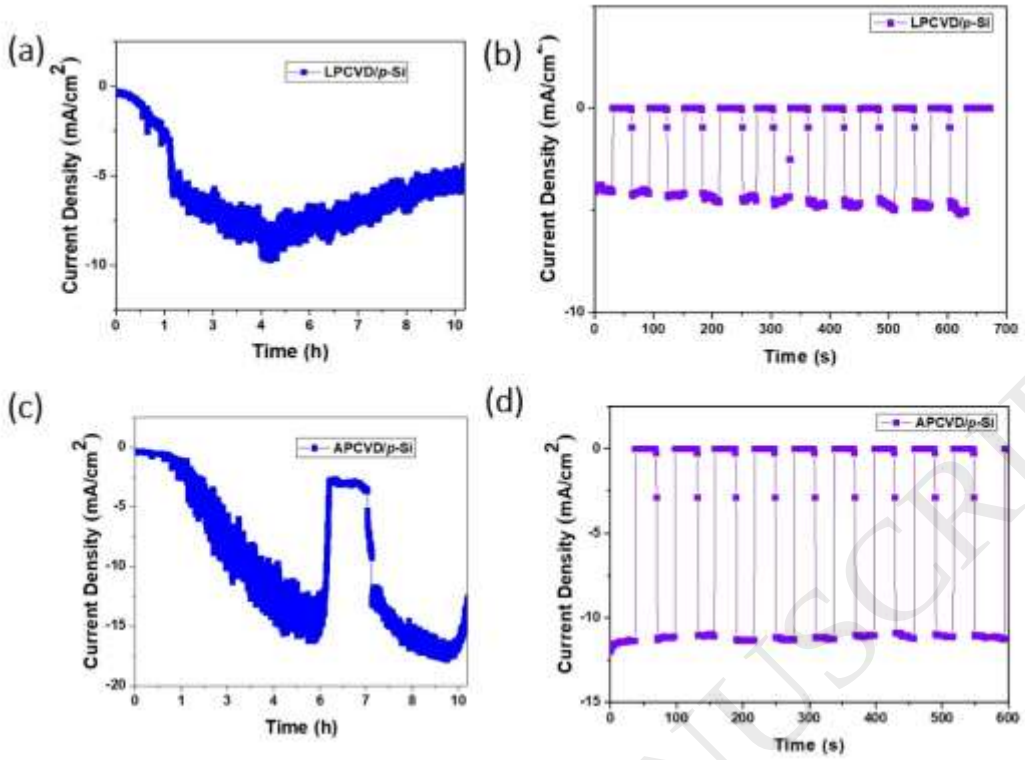

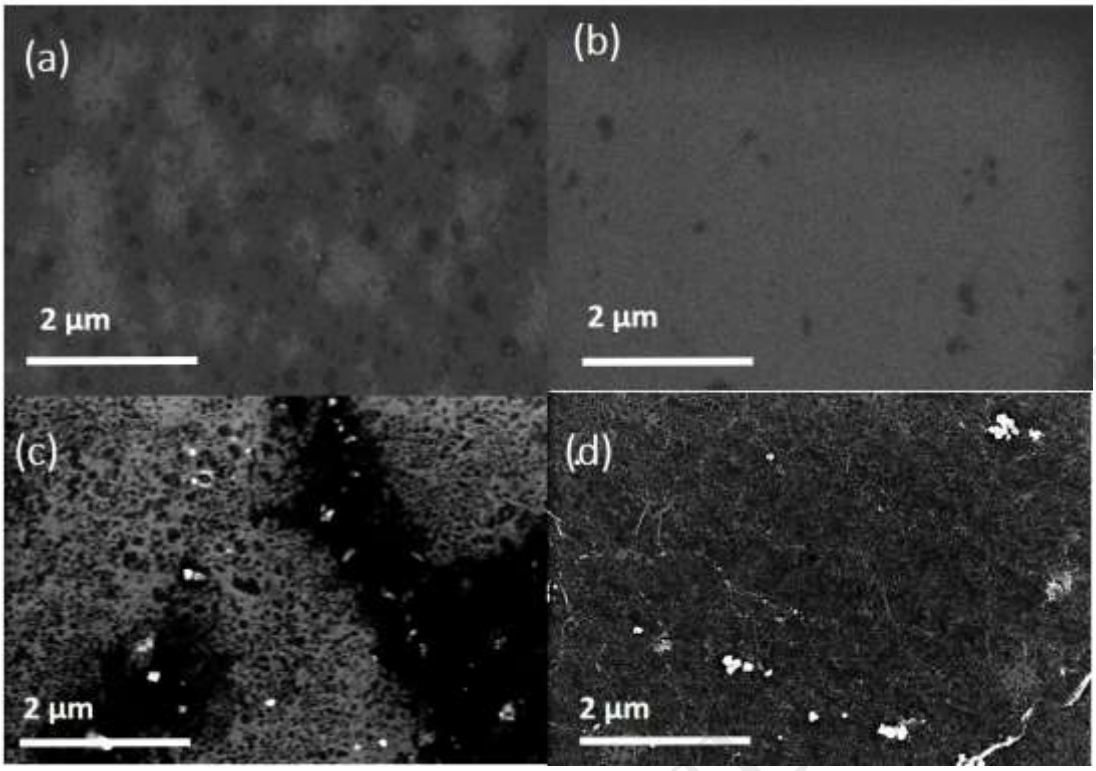

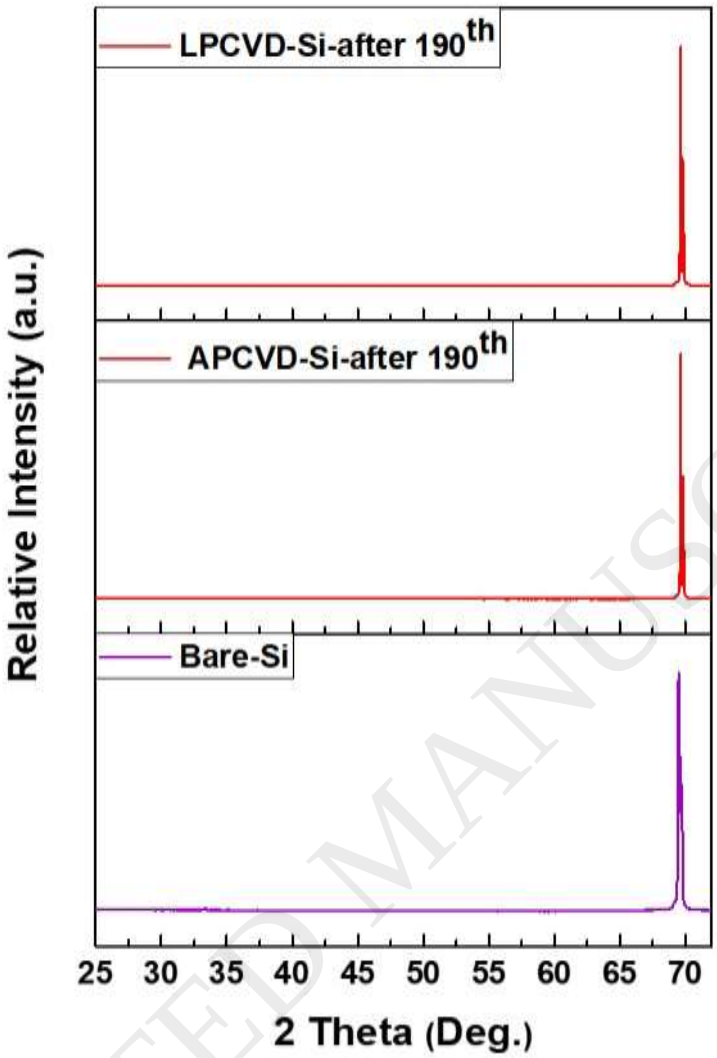

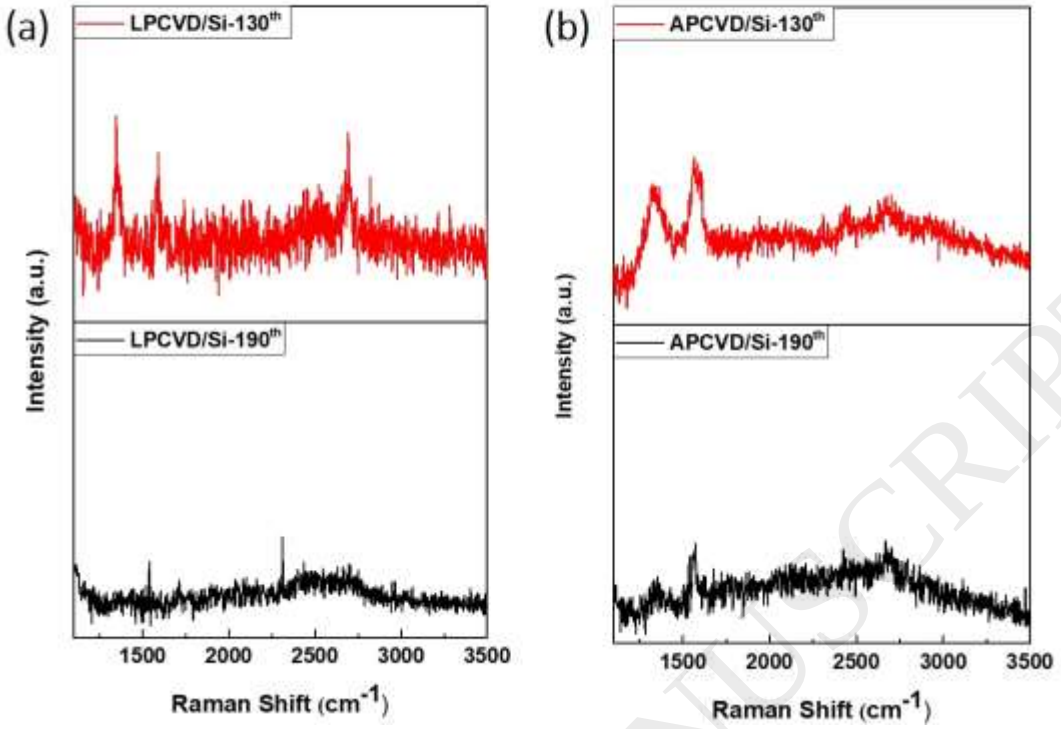

Scheme 1. Schematic illustration of the graphene-modified Si as a photocathode for solar water splitting.